Integrated modelling of island growth, stabilization and mode locking: consequences for NTM control on ITER

2012 Plasma Phys. Control. Fusion 54 094003

(http://iopscience.iop.org/0741-3335/54/9/094003)

Plasma Phys. Control. Fusion **54** (2012) 094003 (9pp) doi:10.1088/0741-3335/54/9/094003

Integrated modelling of island growth, stabilization and mode locking: consequences for NTM control on ITER

H van den Brand[1,3], M R de Baar[2,3], N J Lopes Cardozo[1] and E Westerhof[3]

[1] Fusion Science and Technology Group, Eindhoven University of Technology, PO Box 513, 5600 MB Eindhoven, The Netherlands
[2] Control Systems Technology Group, Eindhoven University of Technology, PO Box 513, 5600 MB Eindhoven, The Netherlands
[3] FOM Institute DIFFER-Dutch Institute for Fundamental Energy Research, Association EURATOM-FOM, Trilateral Euregio Cluster, PO Box 1207, 3430 BE Nieuwegein, The Netherlands

E-mail: E.Westerhof@differ.nl

Received 29 November 2011, in final form 28 April 2012
Published 17 August 2012
Online at stacks.iop.org/PPCF/54/094003

Abstract
Full suppression of neoclassical tearing modes (NTMs) using electron cyclotron current drive (ECCD) should be reached before mode locking (stop of rotation) makes suppression impossible. For an ITER scenario 2 plasma, the similar time scales for locking and island growth necessitate the combined modelling of the growth of the mode and its slow down due to wall induced drag. Using such a model, the maximum allowed latency between the seeding of the mode and the start of ECCD deposition and maximum deviation in the radial position are determined. The maximum allowed latency is determined for two limiting models for island growth; the polarization model with $w_{\mathrm{marg}} = 2$ cm, representing the worst case, and the transport model with $w_{\mathrm{marg}} = 6$ cm, representing the best case. NTMs with seed island widths up to 9.5 cm and 12 cm for the $2/1$ and the $3/2$ NTM, respectively, are suppressible. The maximum allowed latency is 1.05 s and 2.95 s for the $2/1$ and $3/2$ NTM, respectively, for the worst case model. Radial misalignment should not exceed 7–10 mm for the $2/1$ NTM and 5–16 mm for the $3/2$ NTM depending on the model for island growth. As long as the alignment suffices, it does not reduce the maximum allowed latency. Mode locking has serious implications for any real-time NTM control system on ITER that aims to suppress NTMs by ECCD.

(Some figures may appear in colour only in the online journal)

1. Introduction

In order to prove the technical viability of fusion power, the ITER tokamak (major radius $R_0 = 6.2$ m, minor radius $a = 2$ m and elongation $\kappa = 1.7$) is under construction [1]. Plasmas in ITER should maintain a fusion gain $Q = 10$ for 300 s. In order to achieve these goals, plasma instabilities are to be prevented. A particular example is the neoclassical tearing mode (NTM), an MHD instability, which reduces the core temperature, and therefore the fusion yield and can result in the loss of the entire plasma (a disruption) [2]. An NTM is a global magnetic perturbation, with poloidal and toroidal mode numbers m and n, respectively, which create a magnetic island on the resonant flux surface, where the safety factor $q = m/n$. The amplitude of the mode is characterized by the full island width w. The metastable NTM is driven unstable at finite island width due to the loss of local bootstrap current inside the island itself. Electron cyclotron (EC) waves can provide local current through EC resonance heating (ECRH) and current drive (ECCD), replacing the missing bootstrap current in the

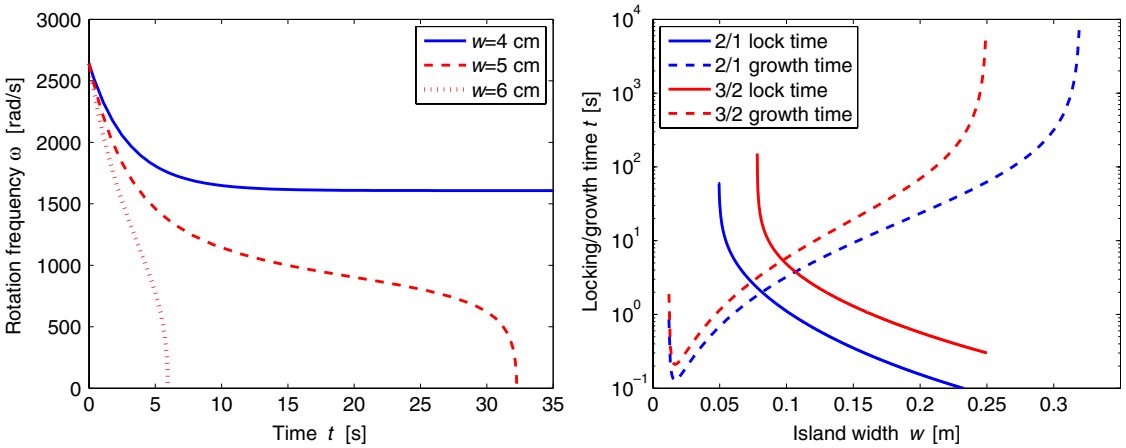

Figure 1. The left figure shows the evolution of the rotation frequency of a $2/1$ mode with a fixed island width w. The solid line shows the rotation frequency for a 4 cm island, which does not lock. The dashed and the dotted lines represent the rotation frequency for a 5 cm and 6 cm island, respectively, which both lock. The right figure shows the locking and island growth time as a function of the fixed island width for the $2/1$ mode (blue) and $3/2$ mode (red). The solid lines are the locking times and the dashed lines are the growth times based on the generalized Rutherford equation (for details see section 2).

island and thereby stabilizing or suppressing the NTM [2, 3]. In ITER, the NTMs with mode numbers $m/n = 2/1$ and $m/n = 3/2$ will degrade the core temperature the most [4].

NTMs are known to rotate toroidally and interaction with the wall results in a slowdown of this rotation [5, 6]. As the mode slows down, it finally locks to the static error field, a situation known as mode locking [7, 8]. In that case, the stabilizing effect of the wall is lost and the mode can grow to still larger amplitudes. In particular, for the case of the $2/1$ mode this generally results in a disruption [9].

ECCD stabilizes the NTM if the current is driven near the island O-point, i.e. the centre of the magnetic island. Current drive near the island X-point, the crossing of the two separatrices of the magnetic island, has a destabilizing effect [10]. Experiments show that for large phase mismatches between island O-point and ECCD the NTM is not fully suppressed [10–12]. In ITER, the four heating and current drive EC upper port launchers are dedicated to the control of NTMs. They are situated in upper ports spanning a range of only 100° in the toroidal angle around the ITER torus [13]. When the mode locks in an unfavourable position, in which ECCD cannot be driven close enough to the O-point, ECCD is unable to stabilize the mode. Therefore, in order to guarantee suppression by ECCD, modes should be suppressed before locking occurs.

La Haye *et al* investigated for which island widths mode locking occurs, using an induced wall drag model adapted from Nave and Wesson [5, 6]. Figure 1, produced using this rotation model (for details see section 2.2), shows that the time it takes for an NTM to lock varies strongly with the island width. The characteristic timescale for island growth is $w/\frac{\mathrm{d}w}{\mathrm{d}t}$, where $\frac{\mathrm{d}w}{\mathrm{d}t}$ is the island growth rate in the absence of ECCD (for details see section 2.1 for the polarization model with $w_{\mathrm{marg}} = 2\,\mathrm{cm}$). Figure 1 shows that the locking time is comparable to the growth time for island widths in the range from 5 to 10 cm. The locking time is neither infinitely fast, which would result in the island width limits by La Haye *et al*, nor is it slow enough to justify neglecting island rotation, as is often done in discussions of the NTM control problem (see, for example, [4]). Consequently, the derivation of control requirements must be based on a model combining the growth of the mode and the evolution of the mode rotation. In an earlier study of a combined model for mode growth and rotation, Ramponi *et al* also noted the fast locking of NTMs in ITER as a consequence of the induced wall drag [14]. Ramponi *et al* suggest to counter the negative effects of mode locking through either an additional external momentum input, in order to keep the mode rotating, or to apply an external magnetic perturbation, to lock the mode in a correct position for efficient suppression by ECCD [14]. Stabilization of NTMs using ECCD is assessed by Ramponi *et al* assuming that such mechanisms are available. Instead, in this paper it is assumed that these mechanisms are lacking, which consequently requires a full suppression of the mode before mode locking occurs.

Using a combined model of mode growth and rotation, this paper investigates how the prevention of mode locking, as a control objective, affects the requirements on a real-time NTM control system. In particular, we look at the maximum allowed latency and the maximum allowed deviation in radial deposition position compared with the island O-point. Under latency we understand the time delay between the island seeding and the start of ECCD deposition at the proper location to suppress the mode. During this time, the control system should (i) detect the mode and identify its position in the plasma and (ii) steer the launcher to position the ECCD at the location of the mode. The maximum allowed latency is the longest time delay that still ensures a full suppression of the island before mode locking and similarly for the maximum allowed deviation in the radial deposition position. In section 2, the generalized Rutherford equation (GRE) and the rotation model are briefly described and the relevant model parameters are specified. In section 3, the model combining the GRE and mode rotation is used to calculate the maximum allowed latency and the required accuracy of ECCD positioning. The results are discussed with a focus on the implications for ITER in section 4. The conclusions of the work are presented in the final section.

2. Model

2.1. Generalized Rutherford equation

The GRE describes the island growth rate $\frac{dw}{dt}$ as a function of island width w, averaged over the equatorial plane high-field side and low-field side, based on an average of the current diffusion equation over the area covering the magnetic island including appropriate corrections in Ohm's law from non-inductively driven currents [2, 15]. Keeping only the most relevant terms within the current context, it can be written as

$$\frac{\tau_r^*}{r_s}\frac{dw}{dt} = r_s\Delta_0' + r_s\Delta_{BS}' + r_s\Delta_{CD}', \tag{1}$$

where r_s is the island position measured as half the flux surface width in the equatorial plane and $\tau_r^* = 0.82\frac{\mu_0\kappa r_s^2}{\eta_{NC}}$ is the resistive time scale of island growth with μ_0 being the permeability of free space and κ the plasma elongation. The neoclassical resistivity is $\eta_{NC} = 2.8\times10^{-8}Z_{eff}(T_e[\mathrm{keV}])^{-3/2}(1-\sqrt{\epsilon})^{-2}$, where Z_{eff} is the effective charge of the plasma ions, T_e the electron temperature in keV and ϵ the inverse aspect ratio, defined as $\epsilon = r_s/R$ with R the major radius [16]. The first term on the right-hand side represents the classical stability index, which is a result of the boundary conditions provided by matching to the ideal MHD perturbation in the region outside the island [15]. The other two terms originate from the loss of the bootstrap current inside the magnetic island and the non-inductively driven current from ECCD, respectively, [2, 17, 18]. A NTM is driven unstable by the bootstrap term and, generally, has a stabilizing classical stability index. As a consequence, NTMs are linearly stable and require a seed island, provided by other MHD instabilities [2]. The negative value of the classical stability index ensures an upper limit for the island width: the saturated island width w_{sat}. At w_{sat} the destabilizing bootstrap growth term is balanced by the classical growth term: $\Delta_0' = -\Delta_{BS}'(w_{sat})$.

The bootstrap term is a consequence of the flattening of the pressure profile inside the island [2]. This results in the loss of the local bootstrap current density j_{BS} inside the magnetic island, such that an island is driven unstable at the rate [19]

$$r_s\Delta_{BS}' = \frac{16\mu_0 L_q r_s j_{BS}}{B_p\pi}\frac{4}{3w} f\left(\frac{w}{w_{marg}}\right), \tag{2}$$

where $L_q = q(\frac{\partial q}{\partial r})^{-1}$ is the q-profile gradient length and B_p the poloidal magnetic field at the rational surface. The function $f(\frac{w}{w_{marg}})$ describes the limitation of the bootstrap growth rate at small island sizes. The precise form of $f(\frac{w}{w_{marg}})$ is still open to debate, but two forms are commonly used in the literature depending on the main mechanism limiting the mode growth at small island widths. In the first model, known as the transport model, the limitation is the result of an incomplete flattening of the pressure profile inside the island, as a consequence of a competition between the finite parallel transport time scale and the perpendicular transport time scale across the island [20]. In this case f is written as

$$f_{tra}\left(\frac{w}{w_{marg}}\right) = \frac{w^2}{w^2 + w_{marg}^2}, \tag{3}$$

where w_{marg} is the island width at which the growth rate has a maximum. In the second model, the polarization model, the limitation of the growth rate at small island widths is a consequence of the so-called ion polarization current, which is a result of the difference between the ion and electron response to island rotation [21, 22]. For the polarization model f is written as

$$f_{pol}\left(\frac{w}{w_{marg}}\right) = 1 - \frac{w_{marg}^2}{3w^2}. \tag{4}$$

The value of w_{marg} for the transport model depends on the ratio of perpendicular to parallel transport, while for the polarization model it depends on the ion banana orbit width [2].

ECCD inside the magnetic island stabilizes the mode by replacing the missing bootstrap current. For a Gaussian driven current density profile, this results in a contribution to the GRE as [17]

$$r_s\Delta_{CD}' = -\frac{16\mu_0 L_q r_s j_{BS}}{B_p\pi}\frac{\pi^{3/2}P}{w_{dep}}\frac{j_{CD,W}}{j_{BS}}F_{CD}\left(w^*, \widehat{x}_{dep}\right), \tag{5}$$

where P is the ECCD power, $j_{CD,W}$ the peak driven current per watt injected power and w_{dep} the full e^{-1} deposition width. The function F_{CD} describes the dependence on ECCD beam width in terms of the relative island width $w^* \equiv w/w_{dep}$ and misalignment in terms of $\widehat{x}_{dep} \equiv \frac{r_{dep}-r_s}{\max(w, w_{dep})}$, where r_{dep} is the deposition position. The fitted expressions describing the separate effects from De Lazzari and Westerhof are used [17, 18]. Strictly speaking, the expressions are averages over one island rotation period and correspond to the limit of fast island rotation. A finite rotation period in combination with a finite collisional time results in an oscillation of the Δ_{CD}' term, which, however, only becomes important for small island widths and rotation periods below 10 Hz [23].

In the derivation of the GRE, it is assumed that magnetic islands are small, compared with the plasma minor radius, and that the plasma is adequately described using constant local plasma parameters. In the classical stability index and the bootstrap growth term finite island width effects are negligible [19]. Degradation of the plasma equilibrium by the island (see for instance [4]) has not been included. In this work, the islands never reach their saturated island size and remain relatively small such that finite island width corrections are negligible. The calculations are stopped either when the island is fully suppressed or when the island locks. Asymmetric islands result in equal current drive efficiency if power is deposited on the island O-point [24]. In this representation of the GRE, the effect of magnetic field curvature, ECRH and the effect of the driven current on the classical stability index are all neglected. Magnetic field curvature results in the Glasser–Greene–Johnson (GGJ) growth term, which is a factor $(\epsilon/q)^2$ smaller than the bootstrap term [25, 26]. Also ECRH is expected to have only a marginal influence on island growth in ITER [17]. The non-inductively driven current can affect the classical stability index only on a resistive diffusion time scale and may be neglected on the short time scales of up to a few seconds occurring in this work, which is mainly determined by the locking time [19, 27].

2.2. Rotation

The rotation model (introduced in the form as used here by La Haye *et al*) assumes that the island width is small, resulting in negligible effects on the global magnetic equilibrium [5]. The island is approximated by a rigid body. Due to viscous coupling with the bulk plasma, the equilibrium toroidal rotation frequency ω_0 in the absence of an island is a balance between momentum input from and loss to the bulk plasma. The rotating magnetic island induces wall currents that slow down the mode rotation, as described by the induced wall drag model from Nave and Wesson [6]. The rate of toroidal rotation change $\frac{d\omega}{dt}$ based on the viscous coupling to the bulk and the induced wall drag is written as [5, 28]

$$\frac{d\omega}{dt} = \left(\frac{\omega_0}{\tau_{E0}} - \frac{\omega}{\tau_E}\right) - \frac{1}{mC_W\tau_{A0}^2\omega\tau_w}\left(\frac{w}{a}\right)^3, \qquad (6)$$

where ω is the toroidal rotation frequency, τ_{E0} is the energy confinement time when no island is present, C_W is a geometrical factor that determines the drag induced by the wall, τ_w is a characteristic resistive time for the wall, τ_{A0} is an Alfvèn time describing the inertia of the magnetic island and a is the plasma minor radius.

This model breaks down at low rotation frequencies $\omega \approx \frac{1}{\tau_w}$ and also does not include the torque from the magnetic error fields, that finally is responsible for the mode locking [7, 8]. The error fields are small and only exert significant torque for small rotation frequencies [8]. The simulation is stopped when the rotation model breaks down. At such low frequencies, the error field should also be taken into account. However, this final phase is expected to be fast in comparison with the full slowing down phase such that its neglect does not introduce a significant error in the estimated locking time. The locking by static error fields for ITER-relevant conditions is studied by Yu and Günter [8].

In (6), the first term between brackets is the viscous coupling term. The two parts of this term represent the equilibrium momentum input, which is assumed to result in a constant rotation frequency in the absence of an island, and the loss of momentum which incorporates degradation of the plasma equilibrium. The confinement degradation by the island is described by a first order correction of the confinement time according to the belt or island model by Chang *et al*, resulting in a decreased energy confinement time τ_E in the presence of an island, described by [29]

$$\tau_E = \frac{\tau_{E0}}{1 + C_M\frac{w}{a}}, \qquad (7)$$

where C_M allows for the confinement degrading effect of the magnetic island on the local momentum input. Strictly speaking the momentum confinement time should be used. For ITER, currently no good estimates exist, because theoretical knowledge of ITER rotation is not yet sufficient to predict the radial rotation profile [30]. Based on extrapolations from current tokamaks, approximating the momentum confinement time with the energy confinement time could result in an underestimation of the momentum confinement time [30]. A larger momentum confinement time would increase the momentum input by viscous coupling with the bulk plasma. As a consequence, mode locking would take a longer time.

The second term in (6) is the wall induced drag term introduced by Nave and Wesson [6]. The wall interaction is assumed to be slow ($\tau_w\omega \gg m$). The scaling of the island inertia, expressed in τ_{A0}, with the island width and plasma minor radius has been explicitly expressed, resulting in a formulation where C_W is a machine-independent parameter.

Table 1. Simulation parameters and values.

		2/1	3/2
Z_{eff} [31]		1.7	1.7
r_s [26]	(m)	1.55	1.3
$j_{BS}(r_s)$ [32]	(kA m^{-2})	73	94
$T_e(r_s)$ [26]	(keV)	5.6	7.6
$B_p(r_s)$ [26]	(T)	0.97	1.07
$L_q(r_s)$ [26]	(m)	0.87	0.88
w_{marg} [4]	(cm)	2–6	2–6
w_{sat} [4]	(cm)	32	25
w_{dep} [19]	(cm)	2.4	3.7
$j_{CD,W}$ [19]	(A m^{-2} W^{-1})	1.32×10^{-2}	1.22×10^{-2}

2.3. Combined model and parameter values

The GRE provides the island width as a function of time and in its current form does not depend on the island rotation frequency. The island width calculated based on this model is used as an input for the rotation model. The models are implemented in MathWorks Simulink and solved using a variable step ordinary differential equation solver (Runge–Kutta fourth order, with fifth order error estimate). Both the island width and the rotation frequency are solved with a relative accuracy of 10^{-6}.

The simulation parameters for ITER scenario 2 are listed in table 1. The values of Bertelli *et al* for the deposition width w_{dep} and the driven current $j_{CD,W}$ are the result of TORBEAM simulations [19, 33]. Values by Urso [26] originate from simulations by Polevoi *et al* [34]. A range 2–6 cm for the marginal island width is used, in accordance with Sauter *et al* [4]. Saturated island widths, as determined by Sauter *et al* based on an evaluation of the GRE terms, are used [4]. Values for the rotation parameters are obtained from La Haye *et al* [28]. C_W and C_M are obtained from fits to DIII-D discharges for an ITER-like plasma equilibrium resulting in ITER-relevant values. The rotation model breaks down at approximately 5.3 rad s^{-1} and 8 rad s^{-1} for the 2/1 and 3/2 NTM, respectively.

The highest efficiency for stabilization of both the 2/1 and the 3/2 NTM is obtained with beams injected from the lower steering mirrors (LSMs) of the EC upper port launcher [19]. With four ECCD launchers and four beams per LSM, a total of 16 beams with a combined injected power of 13.3 MW can be focused on the NTM [35]. In the rest of this paper, ECCD is assumed to be continuous wave and perfectly aligned on the NTM resonant flux surface, unless stated otherwise. As a result of the continuous wave ECCD, no measurement and feedback based on the island phase is required.

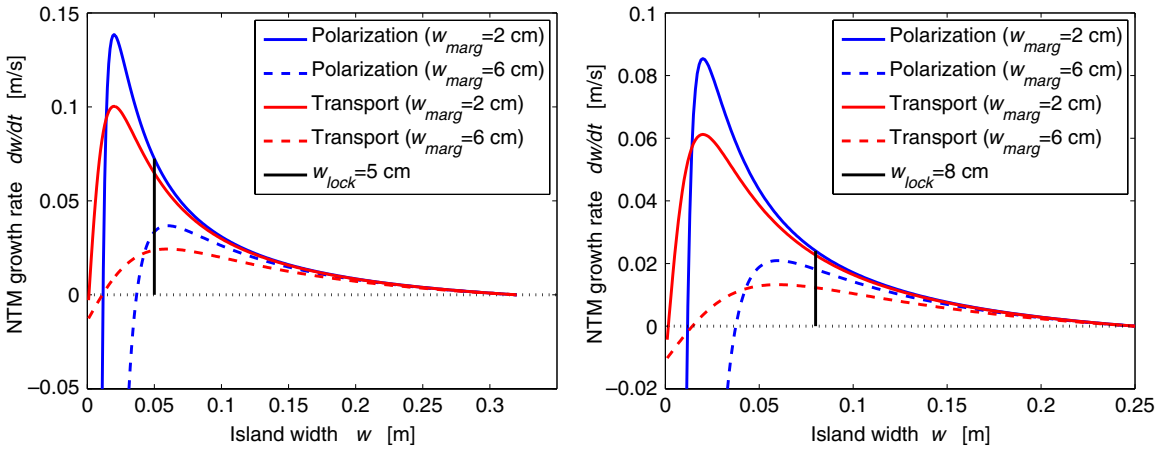

(a) 2/1 NTM **(b)** 3/2 NTM

Figure 2. Plot of the GRE for the 2/1 and 3/2 NTM. Polarization (blue) and transport (red) models are both plotted with marginal island widths w_{marg} of 2 cm (solid lines) and 6 cm (dotted lines). The solid vertical black lines indicate locking island widths w_{lock}, which are 5 cm and 8 cm for the 2/1 and 3/2 NTM, respectively [28].

3. Results

3.1. Bootstrap models

The two bootstrap models and the minimum and maximum values of the marginal island width provide four different values for the island growth rate $\frac{\mathrm{d}w}{\mathrm{d}t}$ at a given island width w. The dependence of the island growth rate on the island width, in the absence of ECCD, is plotted for these four different cases in figures 2(*a*) and (*b*) for the 2/1 and 3/2 NTM, respectively. A solid vertical line in the figures indicates where the island width equals the locking island width w_{lock}, as determined by La Haye *et al* [28].

Fast island growth results in larger islands and consequently a decreased locking time for island widths above the locking island width w_{lock}. Therefore, the model with the largest growth rate for widths larger than the locking island width will result in the shortest locking times and, conversely, the model with the lowest growth rate results in the longest locking times. The locking time results in a limit on the maximum allowed latency between island seeding and the start of ECCD deposition. Based on this consideration and figure 2, the polarization model with $w_{\mathrm{marg}} = 2\,\mathrm{cm}$ results in the shortest maximum allowed latencies and the transport model with $w_{\mathrm{marg}} = 6\,\mathrm{cm}$ results in the longest maximum allowed latencies. The other models provide intermediate results.

As the rotation frequency drops, the locking island width decreases as well. In this case the polarization model with $w_{\mathrm{marg}} = 2\,\mathrm{cm}$ remains the hardest to stabilize for island widths larger than w_{marg}. However, for even smaller island widths the polarization model predicts island width decline without ECCD. Seed island widths smaller than 2 cm are therefore excluded from the simulations. Island widths smaller than 2 cm result in an increased maximum allowed latency for the transport models and therefore do not impose more stringent requirements on the maximum allowed latency.

The maximum allowed latency does not relate to the required energy or ECCD power for stabilization in a straightforward way. The required energy or power determines whether a rotating NTM can be stabilized (given a sufficiently short delay), while the maximum allowed latency determines whether the stabilization is fast enough to avoid mode locking.

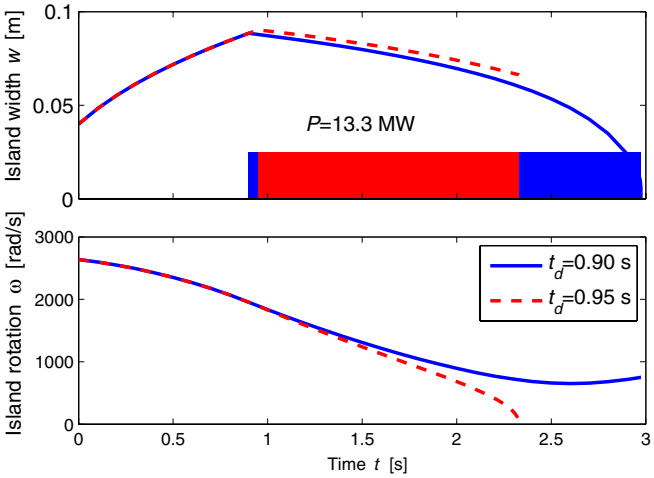

Figure 3. Simulation of the island width and rotation frequency of a 2/1 NTM with the polarization model with $w_{\mathrm{marg}} = 2\,\mathrm{cm}$. At $t = 0\,\mathrm{s}$ a seed island with a width $w_{\mathrm{seed}} = 4\,\mathrm{cm}$ is formed and starts to grow. The start of the deposition is 0.90 s and 0.95 s after island seeding, which is depicted by the solid and dashed curve, respectively.

3.2. Island width and rotation frequency

The island width and the rotation frequency as a function of time are shown in figure 3 for a 2/1 NTM. An island of 4 cm is seeded at $t = 0\,\mathrm{s}$ with an equilibrium rotation frequency of 2640 rad s^{-1} and starts to grow in width and decrease in rotation frequency. Island growth is described by the polarization model with $w_{\mathrm{marg}} = 2\,\mathrm{cm}$.

The time delay t_{d} between seeding and ECCD deposition start is varied in steps of 50 ms. As the delay is increased, a point is reached where the rotation frequency becomes zero before the mode is fully suppressed. When this happens the

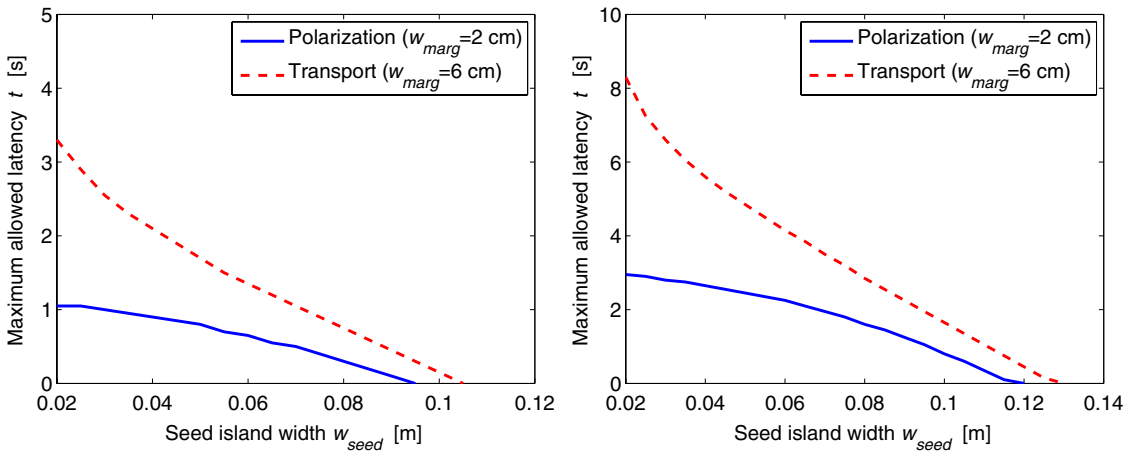

(a) 2/1 NTM **(b)** 3/2 NTM

Figure 4. Maximum allowed latency between seeding of the mode and ECCD deposition start. The plots show both the polarization (solid line) and the transport model (dashed line) with marginal island widths w_{marg} of, respectively, 2 and 6 cm for the 2/1 and 3/2 NTM.

mode may lock in an unfavourable phase such that ECCD can no longer suppress the mode. In figure 3, full suppression is not possible with $t_{\mathrm{d}} \geqslant 0.95$ s, but with a delay $t_{\mathrm{d}} = 0.9$ s, the mode can be suppressed before locking. Therefore, for these settings, the total latency introduced between island seeding and the start of ECCD deposition on the mode should be smaller than or equal to 0.9 s. The longest time delay for which a mode is suppressed without locking, is called the maximum allowed latency.

3.3. Maximum allowed latency and deviation in radial position

In the previous section, the maximum allowed latency is derived from time-dependent simulations of the island width and the rotation frequency. Due to the strong dependence of locking time on island width, the maximum allowed latency should be determined for all seed island widths individually. The polarization model with $w_{\mathrm{marg}} = 2$ cm and the transport model with $w_{\mathrm{marg}} = 6$ cm provide, respectively, the lower and upper limits to the maximum allowed latency. Figure 4 shows the maximum allowed latency for both models and both the 2/1 and 3/2 NTMs as a function of seed island width. The maximum allowed latency is determined with an accuracy of 50 ms.

The polarization and the transport model differ not only in the maximum allowed latency value, but also on the dependence of the value on the seed island width. The curve for the polarization model is flatter than the transport model curve, resulting from the localized peak in the island growth rate. The transport curve, on the other hand, is affected by the much broader peak in the island growth rate, resulting in a steeper curve.

Figure 4 shows that the locking island widths w_{lock} of 5 and 8 cm for the 2/1 and 3/2 NTMs, as put forward by La Haye *et al*, are not absolute limits [28]. Even modes that have grown significantly larger or that are seeded at a larger island width than the locking width can still be fully suppressed before the mode locks provided that the maximum allowed latency is not exceeded. The maximum allowed latency is seen to reduce to zero for a 9.5 cm island in the case of the 2/1 mode and for a 12 cm island in the case of a 3/2 mode. Full suppression of the NTMs requires the control system latency to be well below the maximum allowed latency of 1.05 s and 2.95 s for the 2/1 and 3/2 modes, respectively, with the polarization model. Increasing the ECCD power to 20 MW, results in an increase in the maximum allowed latency by 300 ms and 800 ms for the 2/1 and 3/2 modes, respectively, for the polarization model. For both modes, the maximum allowed latency reaches zero for seed island widths 1.5 cm larger than with 13.3 MW. This improvement shows approximately linear scaling with the available ECCD power, as expected based on the ECCD island growth rate. The effect of modulation on the maximum allowed latency is less than 100 ms and 350 ms for the 2/1 and 3/2 modes, respectively. In this case, the phase of the ECCD is assumed to match the island phase perfectly. A phase mismatch reduces the efficiency and could, for large mismatches, even lead to destabilization.

The expressions for the ECCD efficiency as a result of misalignment from De Lazzari *et al* are used to evaluate the GRE for different misalignments $x_{\mathrm{dep}} = r_{\mathrm{dep}} - r_{\mathrm{s}}$ [24]. For full suppression of the mode, it is required that the island width growth rate is negative for all island widths. Based on this criterion, the maximum allowed deviation in the radial position is 7–10 mm for the 2/1 NTM and 5–16 mm for the 3/2 NTM. The limiting values are given by the polarization model with a marginal island width of 2 cm and the transport model with 6 cm, respectively. La Haye *et al* derived values for the misalignment based on the criterion that the GRE should be negative for island widths larger than the locking width (5 cm and 8 cm for 2/1 and 3/2 respectively) [28]. This results in slightly larger estimates of the allowed misalignment (15 mm and 25 mm for 2/1 and 3/2 respectively), because the misalignment results in the largest reduction in ECCD efficiency for small island widths [28]. At the maximum allowable deviation, the simulations show a negligible decrease in maximum allowed latency. This is explained by the dependence of the efficiency on island widths. Only for small

island widths does the effect of misalignment on the ECCD efficiency become significant. However, for small islands the decrease in rotation frequency is small, leading to a negligible influence on the time it takes for islands to lock. Furthermore, small enough islands maintain a finite rotation frequency. Consequently, the time it takes for a growing island to lock, in the absence of ECCD, is unaffected by small islands, resulting in a negligible contribution to the related maximum allowed latency.

4. Discussion

Based on the model in which the a rotation model and the GRE are combined, the maximum allowed latency and deviation in radial position are derived for ITER scenario 2 parameters. The significance of these values depends on the chosen strategy for the NTM control system on ITER. In this section, the significance of the maximum allowed latency and radial deviation are considered for different choices of the control strategy, actuators and detectors. These three aspects of the control system, though being a necessary part of an integrated system, are treated separately in the following paragraphs.

A straightforward control strategy relies on only acting when an island is present: detect the mode, position the suppression mechanism and suppress the mode, repeating the scheme for every new occurrence of a mode. Most control schemes rely on this strategy with EC waves for mode suppression [10, 36–38]. The maximum allowed latency and the radial deviation are derived for this strategy. However, one could also influence the plasma profile using preemptive methods, in order to prevent the formation of NTMs altogether [4]. On the opposite side of the spectrum, islands can be actively tracked and kept at a small size using continued stabilization of the mode [14, 39]. Alternatively, one could drop the condition of suppression before mode locking and provide active or passive mechanisms to influence the mode phase [14].

ECCD is considered the main actuator for mode stabilization, suppression and preemptive control on ITER. Using mirrors, ECCD is deposited at the right position. Recent work by Collazos *et al* reports a steering mirror angle settling time of 2.5 s for angles equivalent to switching between different mode positions [40]. This settling time is longer than the maximum allowed latency for the 2/1 NTM. Therefore, without prior knowledge of the mode position, it is impossible to fully suppress the 2/1 mode before mode locking. This can be remedied by increasing the steering mirror performance or by making sure the required angle variation is small due to *a priori* knowledge on the mode location. The control strategies based on preemptive stabilization and island tracking are not hampered by the mirror angle settling time, because they exploit *a priori* knowledge and require only small variations in the mirror angles, respectively.

The incorporation of a second actuator in the control loop could also drastically improve the possibilities of stabilization. If the phase of the island can be controlled, it can be changed to ensure maximum stabilization efficiency of ECCD [14]. In this case mode locking is no longer a direct problem. Using additional magnetic fields, it should be possible to make the mode always lock in a phase that makes ECCD possible and efficient. This could be achieved either by a static error field or by active control with magnetic coils. Previous studies investigated NTM locking to error fields, finding thresholds for locking to static error fields and increased island suppression with modulated RF current in phase with external helical error fields [7, 8, 14].

The radial misalignment should be smaller than the maximum allowed deviation in the radial position to guarantee full mode suppression. Radial misalignment results from uncertainty in the deposition position of ECCD and the uncertainty in the mode position as detected by a sensor. An accurate determination of the mode position is required if it is used to position the ECCD deposition. Electron cyclotron emission (ECE) and Mirnov coils are the main detectors for the presence of NTM in current experiments [10, 36–38]. However, Mirnov coils are unable to resolve mode positions and the spatial resolution of ECE is limited by broadening effects, making it an open issue whether the mode position can be accurately determined [41]. Therefore, one of the two measurements needs to be supplemented with plasma equilibrium information to determine the mode position. This requires very high accuracy of measurements used in the equilibrium reconstruction and equally high accuracy in the equilibrium reconstruction itself. Using a different control strategy can relax the accuracy requirements. For instance, tracking of small islands does not require full suppression and can therefore tolerate a higher radial misalignment. Experiments have also been carried out that use the same line-of-sight for ECE and ECCD, thereby compensating the error made in the determination of the mode position (i.e. ECE frequency of the island) by an exactly compensating error in ECCD positioning [42]. Note that detection, especially if it entails reconstruction of the plasma equilibrium, contributes to the control system latency as well.

5. Conclusions

In this paper, we have modelled the combined evolution of the island width and rotation frequency of NTMs in ITER from their initial seeding until their full suppression by ECCD or their locking. Although the rotation model used does not include a proper description of the final locking of the mode to the error field, this is expected to introduce an insignificant uncertainly in the estimate of the time between seeding and mode locking [8]. The main purpose of this work was to find the maximum allowed latency between the seeding of the NTM and the start of the ECCD such that the mode will be suppressed before it locks. If ECCD cannot be deposited sufficiently close to the island O-point, suppression is impossible. The ITER EC upper port launchers cover only a 100° section in the toroidal angle. Suppression by ECCD of modes locked in an unfavourable position is therefore no longer possible and the locked modes will grow to a larger saturated width. In the present experiments, locking of, in particular, the 2/1 NTM is seen to result in a disruption [9]. This is to be avoided at all costs in ITER.

The parameters used in the calculations are representative for the standard $Q = 10$ H-mode scenario in ITER, also known as ITER scenario 2 (see table 1). The calculations assume a continuous wave ECCD power of 13.3 MW injected into the plasma, which corresponds to the use of all 16 beam lines, from a single set of steering mirrors, at 1 MW originating from each gyrotron. The calculations show that the maximum allowed latency depends strongly on seed island width and on the marginal island width determined by the small island physics. When the seed island width exceeds 9.5 cm for the 2/1 or 12 cm for the 3/2 mode, locking becomes inevitable even when the ECCD is switched on immediately: i.e. the maximum allowed latency decreases to zero at these seed island widths. At a seed island width of only 2 cm the maximum allowed latency for the 2/1 mode is 1.05 s for the polarization model with $w_{\mathrm{marg}} = 2$ cm. The corresponding maximum latency for the case of the 3/2 NTM is 2.95 s. The maximum allowed latency scales almost linearly with ECCD power as expected based on the ECCD growth rate. The effect of modulation on the maximum allowed latency is about 10% for both modes. Note that for modulated ECCD, a possible mismatch between ECCD and island phase is not taken into account.

In addition, this work has confirmed that the ECCD should be localized within about 1 cm from the radial position of the island O-point [28]. For larger deviations full mode suppression becomes impossible. The accuracy requirement is mainly a result of the radial alignment needed for full suppression of small islands. A possible mismatch has, however, little effect on the maximum allowed latency to prevent mode locking, which depends on the total time it takes to suppress the mode from an initial width of about 10 cm to just below the locking width (i.e. about 5 cm for the 2/1 mode). During this time a 1 cm mismatch will have little effect.

The total latency in a real-time NTM control system will consist of the sum of the times required (i) to identify the presence of a mode and its location in the plasma and (ii) to calculate the appropriate steering angle to deposit the ECCD at this location and to actively steer the mirror to this required angle. Only the latter process, the steering of the ITER ECRH mirrors in the upper port launchers, may take already up to 2.5 s which is more than the maximum allowed latency for the 2/1 mode in almost all of the relevant parameter space [40].

In conclusion, mode locking has serious implications for any real-time NTM control system on ITER that aims to suppress NTMs by ECCD. The total latency in such a system should be reduced well below 1 s. Using extra actuators for control of the island phase or completely different control strategies (island tracking, preemptive stabilization) are options if the latency and radial accuracy requirements cannot be met for a control system relying on full mode suppression using ECCD. Using additional actuators for phase control has been proposed by Ramponi *et al* [14].

Acknowledgments

The work in this paper has been performed within the framework of the NWO-RFBR Centre of Excellence on Fusion Physics and Technology (grant 047.018.002). This work, supported by the European Communities under the contract of association between EURATOM-FOM, was carried out within the framework of the European Fusion Program. The views and opinions expressed herein do not necessarily reflect those of the European Commission.

References

[1] Shimada M *et al* 2007 Chapter 1: Overview and summary *Nucl. Fusion* **47** S1
[2] La Haye R J 2006 Neoclassical tearing modes and their control *Phys. Plasmas* **13** 055501
[3] Prater R 2004 Heating and current drive by electron cyclotron waves *Phys. Plasmas* **11** 2349–76
[4] Sauter O, Henderson M A, Ramponi G, Zohm H and Zucca C 2010 On the requirements to control neoclassical tearing modes in burning plasmas *Plasma Phys. Control. Fusion* **52** 025002
[5] La Haye R J, Prater R, Buttery R J, Hayashi N, Isayama A, Maraschek M E, Urso L and Zohm H 2006 Cross-machine benchmarking for ITER of neoclassical tearing mode stabilization by electron cyclotron current drive *Nucl. Fusion* **46** 451
[6] Nave M F F and Wesson J A 1990 Mode locking in tokamaks *Nucl. Fusion* **30** 2575
[7] Lazzaro E and Nave M F F 1988 Feedback control of rotating resistive modes *Phys. Fluids* **31** 1623–9
[8] Yu Q and Günter S 2008 Locking of neoclassical tearing modes by error fields and its stabilization by rf current *Nucl. Fusion* **48** 065004
[9] Sauter O *et al* 1997 Beta limits in long-pulse tokamak discharges *Phys. Plasmas* **4** 1654–64
[10] Isayama A *et al* and the JT-60 team 2009 Neoclassical tearing mode control using electron cyclotron current drive and magnetic island evolution in JT-60U *Nucl. Fusion* **49** 055006
[11] Maraschek M, Gantenbein G, Yu Q, Zohm H, Günter S, Leuterer F and Manini A 2007 Enhancement of the stabilization efficiency of a neoclassical magnetic island by modulated electron cyclotron current drive in the ASDEX Upgrade Tokamak *Phys. Rev. Lett.* **98** 025005
[12] Hegna C C and Callen J D 1997 On the stabilization of neoclassical magnetohydrodynamic tearing modes using localized current drive or heating *Phys. Plasmas* **4** 2940–6
[13] ITER Organisation 2007 Project Integration Document (ITER_D_2234RH) Version 3.0, January 2007
[14] Ramponi G, Lazzaro E and Nowak S 1999 On the stabilization of neoclassical tearing modes by electron cyclotron waves *Phys. Plasmas* **6** 3561–70
[15] Rutherford P H 1973 Nonlinear growth of the tearing mode *Phys. Fluids* **16** 1903–8
[16] Wesson J 2004 *Tokamaks* 3rd edn (Oxford: Clarendon)
[17] De Lazzari D and Westerhof E 2009 On the merits of heating and current drive for tearing mode stabilization *Nucl. Fusion* **49** 075002
[18] De Lazzari D and Westerhof E 2010 On the merits of heating and current drive for tearing mode stabilization *Nucl. Fusion* **50** 079801
[19] Bertelli N, De Lazzari D and Westerhof E 2011 Requirements on localized current drive for the suppression of neoclassical tearing modes *Nucl. Fusion* **51** 103007
[20] Fitzpatrick R 1995 Helical temperature perturbations associated with tearing modes in tokamak plasmas *Phys. Plasmas* **2** 825–38

[21] Waelbroeck F L, Connor J W and Wilson H R 2001 Finite Larmor-radius theory of magnetic island evolution *Phys. Rev. Lett.* **87** 215003
[22] Wilson H R, Connor J W, Hastie R J and Hegna C C 1996 Threshold for neoclassical magnetic islands in a low collision frequency tokamak *Phys. Plasmas* **3** 248–65
[23] Ayten B 2011 private communication
[24] De Lazzari D and Westerhof E 2011 The role of asymmetries in the growth and suppression of neoclassical tearing modes *Plasma Phys. Control. Fusion* **53** 035020
[25] Glasser A H, Greene J M and Johnson J L 1976 Resistive instabilities in a tokamak *Phys. Fluids* **19** 567–74
[26] Urso L 2009 Modelling and experiments on NTM stabilisation at ASDEX Upgrade *PhD Thesis* Ludwig-Maximilians-Universität München available at http://nbn-resolving.de/urn:nbn:de:bvb:19-106262
[27] Westerhof E 1990 Tearing mode stabilization by local current density perturbations *Nucl. Fusion* **30** 1143
[28] La Haye R J, Ferron J R, Humphreys D A, Luce T C, Petty C C, Prater R, Strait E J and Welander A S 2008 Requirements for alignment of electron cyclotron current drive for neoclassical tearing mode stabilization in ITER *Nucl. Fusion* **48** 054004
[29] Chang Z and Callen J D 1990 Global energy confinement degradation due to macroscopic phenomena in tokamaks *Nucl. Fusion* **30** 219
[30] Tala T *et al* and JET-EFDA Contributors 2007 Toroidal and poloidal momentum transport studies in tokamaks *Plasma Phys. Control. Fusion* **49** B291
[31] Shimada M *et al* ITER JCT and Home Teams 2000 Physics Design of ITER-FEAT *J. Plasma Fusion Res. Ser.* **3** 77–83
[32] Ramponi G, Farina D, Henderson M A, Poli E, Sauter O, Saibene G, Zohm H and Zucca C 2008 Physics analysis of the ITER ECW system for optimized performance *Nucl. Fusion* **48** 054012
[33] Poli E, Peeters A G and Pereverzev G V 2001 TORBEAM, a beam tracing code for electron-cyclotron waves in tokamak plasmas *Comput. Phys. Commun.* **136** 90–104
[34] Polevoi A R, Medvedev S Y, Mukhovatov V S, Kukushkin A S, Murakami Y, Shimada M and Ivanov A A 2002 ITER confinement and stability modelling *J. Plasma Fusion Res. Ser.* **5** 82–7
[35] Henderson M A *et al* 2008 Overview of the ITER EC upper launcher *Nucl. Fusion* **48** 054013
[36] Manini A *et al* 2007 Development of a feedback system to control MHD instabilities in Asdex Upgrade *Proc. 24th Symp. on Fusion Technology—SOFT-24 (Warsaw) Fusion Eng. Des.* **82** 995–1001
[37] Humphreys D A, Ferron J R, La Haye R J, Luce T C, Petty C C, Prater R and Welander A S 2006 Active control for stabilization of neoclassical tearing modes *Phys. Plasmas* **13** 056113
[38] Hennen B A, Westerhof E, Nuij P W J M, Oosterbeek J W, de Baar M R, Bongers W A, Bürger A, Thoen D J, Steinbuch M and the TEXTOR Team 2010 Real-time control of tearing modes using a line-of-sight electron cyclotron emission diagnostic *Plasma Phys. Control. Fusion* **52** 104006
[39] Hennen B A, Westerhof E, Nuij P W J M, de Baar M R and Steinbuch M 2012 Systematic design of a tearing mode controller for TEXTOR *Nucl. Fusion* **52** 074009
[40] Collazos A, Bertizzolo R, Chavan R, Dolizy F, Felici F, Goodman T P, Henderson M A, Landis J-D and Sanchez F 2010 Progress on the ITER H&CD EC upper launcher steering-mirror control system *IEEE Trans. Plasma Science* **38** 441–7
[41] Austin M E, Phillips P E, Rowan W L, Beno J, Liu H-P, Ouroua A, Ellis R F, Harvey R W, Hubbard A E, Taylor G and Johnson D W 2008 ITER ECE: plans and challenges *EC-15 Joint Workshop on ECE and ECRH (Yosemite National Park, CA)* P2.170
[42] Bongers W A *et al* and TEXTOR Team 2009 Magnetic island localization for NTM control by ECE viewed along the same optical path of the ECCD beam *Fusion Sci. Technol.* **55** 188–203